# Event Horizon Telescope observations as probes for quantum structure of astrophysical black holes

Steven B. Giddings[1] and Dimitrios Psaltis[2]

[1]Department of Physics, University of California, Santa Barbara, California 93106, USA
[2]Departments of Astronomy and Physics, University of Arizona, Tucson, Arizona 85721, USA

(Received 3 July 2016; published 19 April 2018)

The need for a consistent quantum evolution for black holes has led to proposals that their semiclassical description is modified not just near the singularity, but at horizon or larger scales. If such modifications extend beyond the horizon, they influence regions accessible to distant observation. Natural candidates for these modifications behave like metric fluctuations, with characteristic length scales and timescales set by the horizon radius. We investigate the possibility of using the Event Horizon Telescope to observe these effects, if they have a strength sufficient to make quantum evolution consistent with unitarity, without introducing new scales. We find that such quantum fluctuations can introduce a strong time dependence for the shape and size of the shadow that a black hole casts on its surrounding emission. For the black hole in the center of the Milky Way, detecting the rapid time variability of its shadow will require nonimaging timing techniques. However, for the much larger black hole in the center of the M87 galaxy, a variable black-hole shadow, if present with these parameters, would be readily observable in the individual snapshots that will be obtained by the Event Horizon Telescope.

DOI: 10.1103/PhysRevD.97.084035

## I. INTRODUCTION

The discovery of Hawking radiation [1] yields a logical contradiction when one tries to account for quantum information absorbed by a black hole: this information cannot escape, cannot be destroyed, and cannot be preserved after the black hole evaporates. (For reviews, see [2–7].) This situation appears to represent a fundamental conflict between the principles underpinning local quantum field theory: the principles of quantum mechanics, relativity, and locality. Therefore, while it has long been believed that the vicinity of the horizon is well-described by classical general relativity, since curvatures are expected to be small there, many theorists who study quantum evolution of black holes have now concluded that there must be modifications to their description via local quantum field theory, and that in order to resolve the conflict, these modifications must extend *at least to horizon scales*.

A variety of proposals have been made for such new physics. One possibility is new *hard* structure outside of, and replacing, the horizon, e.g., if a new kind of massive black-hole remnant [8] forms, placing the information outside the horizon, while the black hole is still large. Variants of this basic scenario include that of fuzzballs [9], where higher-dimensional string theory configurations are proposed to replace the smooth four-dimensional geometry outside the horizon, or that of gravastars [10]. More recently, it has similarly been proposed [11] that semiclassical geometry breaks down within a Planck distance $l_{\rm Pl}$ of the horizon, forming a "firewall" that destroys all infalling matter. So far, however, there is no concrete theoretical description of any of these scenarios for Schwarzschild or Kerr black holes in terms of more fundamental theory. (Other scenarios propose even more radical modification of the structure of spacetime, extending to greater distances from a black hole [12].)

Such a hard (high momentum) quantum structure for black holes represents a major departure from the familiar spacetime description of black holes and, in particular, greatly alters the description of the infalling observer. Moreover, any theory that accounts for it will apparently have to explain very disparate scales. To take the extreme example, the firewall scenario assumes that new physics alters the classical geometry of a black hole not just at the center of the black hole but all the way to the horizon, *but* the modification extends at most a distance $\sim l_{\rm Pl}$ (or some other microscopic cutoff scale) from the horizon. This appears to require an extreme fine-tuning for a large black hole.

Indeed, to begin to quantify differences in proposals, one may define a scale $R_a$ which characterizes how far outside the would-be horizon the semiclassical geometry is significantly modified; for the firewall proposal, one thus has $R_a \sim l_{\rm Pl} \ll R_{\rm S}$, where $R_{\rm S}$ is the Schwarzschild radius of the black hole.[1] Another characteristic scale [13] is the scale $L$

[1]For simplicity this paper treats nonrotating black holes as a test case, though our results are expected to generalize to the rotating case.

 

on which such departures from the semiclassical geometry vary. Clearly $L \leq R_a$—one could have a "quantum atmosphere" extending to $R_a$, but with "harder" (higher momentum) variation on shorter scales. For example, in the fuzzball context [9], it has been suggested [14] that $L$ could be the size of the extra dimensions of string theory, i.e., microscopic, but there is no clear prediction for $R_a$, which could be much larger.

If we want to avoid such a violent breakdown of the spacetime, e.g., as seen by the infalling observer, and the fine-tuning we have described, the scales $L$ and $R_a$ should become large for large black holes. For example, they could scale as $R_a \sim R_S^p$, $L \sim R_S^q$, for some $p, q > 0$, so the momentum scales of perturbations seen by infalling observers become soft for a large enough black hole. References [15–17] proposed this alternative: the new physics that produces quantum structure on black holes is not finely tuned so that this structure ends abruptly at the horizon, but can instead extend to a macroscopic distance outside, and can be "soft," or "nonviolent." Indeed, if the necessary new physics leads to quantum modifications to the standard description over distances $\sim R_S$ (reaching from the center of the black hole to the horizon), the simplest alternative is that this physics is characterized by this single scale, so that $p = q = 1$, and the quantum structure extends a distance $\sim R_S$ outside the horizon, rather than ending sharply there.

Any such perturbations to the black-hole metric that extend to a distance $\sim R_S$ can, of course, have observable implications for astrophysical phenomena that originate in the vicinities of black-hole horizons [13,18]. Traditionally, the profiles of iron fluorescence lines and the variability of the x-rays observed from accreting black holes have been used to probe such strong gravitational fields (see discussion in Ref. [19] and references therein). Future missions, such as ESA's Athena, will have the capabilities to trace the time evolution of the fluorescence lines at the dynamical timescale of the innermost stable circular orbit around supermassive black holes [20] and potentially observe such perturbations, if they extend to large enough radius.

In the near future two new approaches to probing the innermost regions of black-hole spacetimes will become available, with the potential of offering probes that are clean of astrophysical complexities. The first involves gravitational wave observations either of coalescing black holes (such as the initial LIGO detection of the source GW150914 [21]) or of extreme mass ratio inspirals [22]. The second involves obtaining images of accreting black holes with horizon-scale resolution using the Event Horizon Telescope [23]. The prospect that gravitational-wave observations could reveal quantum modifications to black-hole dynamics was preliminarily explored in Ref. [24].

The goal of the current paper is to investigate the possible signatures of soft quantum modifications to black-hole metrics that could be imprinted on Event Horizon Telescope observations [13], and thus the sensitivity of these observations to such effects. The benefit of using Event Horizon Telescope observations is that they are probing the stationary spacetimes of supermassive black holes, long after the decay of the classical ringdown modes that were excited during their formation. For the inferred accretion rates of the primary Event Horizon Telescope targets, the amount of mass in the accretion flow is a negligible fraction ($\sim 10^{-9}$) of the mass of the black hole and is not expected to excite any classical spacetime oscillations with amplitudes comparable to those we will be studying here.

In Sec. II, we discuss in more detail the origin and scale of perturbations that might be relevant to large astrophysical black holes. Quantifying their effects on the predicted black-hole images requires performing ray tracing calculations from the image plane of a distant observer down to the horizon of the black hole. For these calculations to be possible, the perturbations to the metric that we consider need to preserve its signature and avoid introducing pathologies outside the horizon (see discussion in Ref. [25]). In Sec. III, we use the formalism of Regge and Wheeler [26] to write a general form of metric perturbations, modulo gauge transformations, and to impose these constraints.

Several earlier studies have explored the effect of stationary modifications to black-hole metrics on the images that will be generated with the Event Horizon Telescope [27–31]. However, introducing time-dependent, nonaxisymmetric perturbations to a spacetime, such as the ones we discuss here, removes all Killing symmetries of the Kerr metric, which have been crucial in improving the performance of most ray tracing algorithms available today. In Sec. IV, we discuss our modifications to our existing algorithm in order to perform ray tracing calculations in a time-dependent, nonaxisymmetric spacetime.

In Sec. IV, we also perform a number of exploratory calculations for different monochromatic perturbations of the black-hole metric and identify the range of parameters that introduce observable effects on the predicted images. In Sec. V, we use simple models for the plasma in the accretion flow around a black hole in order to make concrete predictions of the effects of strong, soft quantum perturbations on the image of accreting black holes. Finally, in Sec. VI, we discuss implications of our results for Event Horizon Telescope observations of the two primary targets, the black hole in the center of the Milky Way and the one in the center of the M87 galaxy.

## II. QUANTUM STRUCTURE FOR ASTROPHYSICAL BLACK HOLES

The ultimate explanation of the quantum structure of a black hole may lie in a fully quantum fundamental description of spacetime. However, we can ask what is a "minimal" departure from the usual description of black holes by semiclassical spacetime and local quantum field

theory that is sufficient to transfer quantum information from the black-hole state to the outgoing radiation, as is apparently necessary to recover unitary quantum-mechanical evolution.[2] One expects that such a minimal departure could be parametrized in terms of new couplings between the "internal" state of the black hole and the quantum fields *near* the black hole—where a quantum field theory description is expected to be approximately valid—and that these couplings transfer the required information [35,36].

A lower bound on the strength of such couplings is thus set by the requirement that they should transfer of order one qubit of information per time $R_S$. This is the necessary transfer rate from a black hole once it has reached the midpoint of its evaporation [37,38], in order to cause a decrease of its von Neumann entropy $S_{vN}$ to zero, rather than the increase to $S_{vN} \sim R_S^2$ predicted by Hawking. In principle, a wide variety of such couplings could accomplish this, e.g., couplings that just produce photon, or graviton, emission.

However, much theoretical work on black holes has been guided by the beautiful story of black-hole thermodynamics, in which the black-hole entropy $S_{BH}$ is proportional to its horizon area, as proposed by Bekenstein and Hawking. If this story is to be preserved, at least approximately, then this imposes a strong constraint on any new dynamics of black holes [11,16,17,33,35,39]. For example, if the information-transferring couplings produce a flux of gravitons from the black hole, in addition to that from the Hawking radiation, then one expects that, if the black hole is brought into thermal equilibrium, it will no longer equilibrate at the Hawking temperature and thus will have entropy different from $S_{BH}$. Moreover, a coupling *just* to gravitons would appear to violate detailed balance and prevent equilibration. In order to preserve an approximation of the standard thermodynamic description, we therefore expect that we should find universal couplings to the fields that can radiate from the black hole, and that these should closely match the Hawking radiation.

In fact, there is a second argument for such universality [13,17,36], based on gedanken experiments [11] involving black-hole mining [40–43]. Here, a cosmic string, or other apparatus, is introduced into the black-hole atmosphere to increase its emission rate. To preserve unitarity, the information transfer out of the black hole must increase commensurately. This suggests the necessity of universal couplings to any possible kind of mining apparatus.

Such universal couplings are most naturally achieved via a coupling between the black-hole state and the stress tensor, e.g., via a term in the action [35,44]

$$\Delta S = \int d^4x \sqrt{-g} H^{\mu\nu}(x) T_{\mu\nu}. \tag{1}$$

[2]The needed information transfer can be sharply characterized in terms of transfer of entanglement [32–34].

Here $H^{\mu\nu}(x)$ is an *operator* that has nontrivial matrix elements between black-hole quantum states and $T_{\mu\nu}$ is the stress tensor of all quantum fields (including the graviton). The integral extends over the support of $H^{\mu\nu}(x)$, which we take to typically extend to radii $\sim R_S + R_a$ from the black-hole center. The universality of (1) nicely mirrors the universal nature of gravity.

In order to produce an average emission spectrum without large departures from the thermal Hawking spectrum, typical matrix elements of $H^{\mu\nu}(x)$ should have time variation on scales $\Delta t \sim R_S$; hard structure can be avoided if the spatial variation is on scales $|\Delta\vec{x}| \sim L$, as described above. Then, the typical magnitude of the elements of $H^{\mu\nu}(x)$ is determined by the condition that they transfer information (or entanglement) at the rate stated above, $\sim 1$ qubit per time $R_S$. In fact, since $H^{\mu\nu}(x)$ is dimensionless, when $R_a \sim L \sim R_S$ the magnitude of $H$ most simply follows from dimensional analysis: we expect [44] a typical size $\langle H^{\mu\nu}\rangle \sim 1$ over the nontrivial range $\Delta x \sim R_a \sim R_S$, as is seen in more detailed analysis. Put more simply, this condition arises from the need for an $\mathcal{O}(1)$ modification to the Hawking radiation, to restore unitary evolution.

If in Eq. (1) we replace the operator $H$ by its average $\langle H^{\mu\nu}\rangle$ over black-hole quantum states, we see that these interactions change the action in the same way as if we were to consider a classical perturbation of the metric, $g_{\mu\nu} \to g_{\mu\nu} + h_{\mu\nu}$, given by (to linear order)

$$h_{\mu\nu}(x) = -2 g_{\mu\kappa} g_{\nu\lambda} \langle H^{\kappa\lambda}(x)\rangle. \tag{2}$$

And if, as the simplest proposal outlined above yields, $\langle H\rangle \sim 1$, the metric perturbations are not parametrically small: the quantum structure is soft, but *strong*. That is, the metric perturbations that suffice to accomplish the needed information transfer are significant—though curvatures near the horizon remain small [44].

To reiterate, the reasoning explained above sets the range $R_a$ outside the horizon over which this *effective* metric perturbation is nonvanishing, the scale $L$ of its variation, and its magnitude. In the absence of a complete theory of quantum gravity, which might allow us to derive the matrix elements of $H^{\mu\nu}$, at least approximately, we can investigate the sensitivity of astrophysical observations to this type of strong, soft effective metric fluctuation by considering relatively general perturbations with these characteristic scales. While we specifically focus in this paper on the case $R_a \sim L \sim R_S$, this obviously could be generalized to describe scenarios with different characteristic scale sizes; one can likewise generalize the couplings (1) to give an effective description of other proposals for black-hole quantum interactions [35,36]—albeit ones that may do more damage to black-hole thermodynamics. In order to stay close to the thermodynamic description, We will specifically focus on perturbations near the thermal frequency, $\omega_T = 1/(8\pi M)$ for a Schwarzschild black hole (unless explicitly

noted otherwise). This also avoids introducing a new scale in the physics. As we note below, it is also true that higher (or lower) frequency perturbations have a smaller effect on black-hole images.

## III. PERTURBED METRICS FOR BLACK HOLES

In this initial study of possible observational effects of quantum structure of black holes, we will focus our attention on nonspinning black holes. In order to minimize artifacts due to coordinate singularities, we will work in a coordinate system that is regular at the future horizon. One such suitable choice is that of ingoing Eddington-Finkelstein coordinates $(v, r, \theta, \phi)$, where the metric $g_{\mu\nu}$ has a form with line element

$$ds^2 = -\left(1 - \frac{R_S}{r}\right) dv^2 + 2dvdr + r^2(d\theta^2 + \sin^2\theta d\phi^2). \quad (3)$$

Unless otherwise noted, we set hereafter $G = c = M = 1$, where $G$, $c$, and $M$ are the gravitational constant, the speed of light, and the mass of the black hole, respectively.

As discussed in Sec. II, we will consider linearized perturbations to this metric, which we will denote by $h_{\mu\nu}$, such that the perturbed metric becomes

$$\tilde{g}_{\mu\nu} = g_{\mu\nu} + h_{\mu\nu}. \quad (4)$$

If these are treated as classical perturbations, not all such perturbations are physical, since some can be removed by a coordinate transformation. Such a transformation, with parameter $\xi^\mu$, produces a linearized change

$$\delta h_{\mu\nu} = \nabla_\mu \xi_\nu + \nabla_\nu \xi_\mu. \quad (5)$$

The analysis of Regge and Wheeler [26] shows that using this freedom, a general perturbation can be reduced to a sum of even and odd perturbations with specific forms.

The even perturbations take the form

$$h_{\mu\nu,\text{even}} = \begin{pmatrix} h_{vv} & h_{rv} & 0 & 0 \\ h_{rv} & h_{rr} & 0 & 0 \\ 0 & 0 & r^2\gamma_{\theta\theta} & 0 \\ 0 & 0 & 0 & r^2\sin^2\theta\gamma_{\theta\theta} \end{pmatrix} \quad (6)$$

and the odd perturbations the form

$$h_{\mu\nu,\text{odd}} = \begin{pmatrix} 0 & 0 & h_{v\theta} & h_{v\phi} \\ 0 & 0 & h_{r\theta} & h_{r\phi} \\ h_{v\theta} & h_{r\theta} & 0 & 0 \\ h_{v\phi} & h_{r\phi} & 0 & 0 \end{pmatrix}. \quad (7)$$

The quantities $h_{vv}$, $h_{rv}$, $h_{rr}$, and $\gamma_{\theta\theta}$ can be arbitrary functions of $(v, r, \theta, \phi)$. Thus they can be expanded in scalar spherical harmonics $Y_{lm}$,

$$h_{\alpha\beta} = \sum_{lm} f^{lm}_{\alpha\beta}(v, r) Y_{lm}, \quad (8)$$

where $\alpha$ and $\beta$ range over values $v$ and $r$, and

$$\gamma_{\theta\theta} = \sum_{lm} f^{lm}_{\theta\theta}(v, r) Y_{lm}. \quad (9)$$

The quantities $h_{va}$ and $h_{ra}$, with $a = \theta, \phi$, can be expanded in terms of vector spherical harmonics,

$$h_{va} = \sum_{lm} f^{lm}_{v}(v, r) Y^a_{lm}, \qquad h_{ra} = \sum_{lm} f^{lm}_{r}(v, r) Y^a_{lm}, \quad (10)$$

given by

$$Y^\theta_{lm} = -\frac{1}{\sin\theta}\partial_\phi Y_{lm}, \qquad Y^\phi_{lm} = \sin\theta\partial_\theta Y_{lm}. \quad (11)$$

The $v$ and $r$ dependence of these perturbations can then be described by expanding the $f^{lm}$ elements in terms of a convenient basis of functions of these coordinates, e.g., plane waves in $v$ and $r$. However, as we have discussed above, we consider the (most conservative) case [15–17] where such perturbations are well-localized within a range of size $R_G$ around the horizon radius $R_S$, where $R_G \sim R_S$. Thus, we specifically consider (sums of) perturbations of the form

$$f^{lm}_A(v, r) = \int d\omega dk \epsilon^{lm}_A(\omega, k) \exp\left[-\frac{(r - R_S)^2}{2R_G^2}\right] exp[-i(\omega v - kr)] \quad (12)$$

parametrized by the functions $\epsilon^{lm}_A(\omega, k)$, where the index $A$ takes on the values $vv, rr, rv, \theta\theta, v, r$. These functions of Fourier variables characterize the spectrum of perturbations that we consider. We may alternately choose to superpose such plane waves so that they localize about a specific time $v$.

In general, such perturbations can lead to pathologies [25]. Specifically, avoiding change in signature of the metric restricts the size of the perturbations. Considering for example the even perturbations, avoiding signature change clearly requires $1 + \gamma_{\theta\theta} > 0$, and the condition

$$\text{Det}\begin{vmatrix} -1 + \frac{R_S}{r} + h_{vv} & 1 + h_{rv} \\ 1 + h_{rv} & h_{rr} \end{vmatrix} < 0, \quad (13)$$

which translates to

$$h_{rr}\left[1 - \frac{R_S}{r} - h_{vv}\right] + (1 + h_{rv})^2 > 0. \quad (14)$$

Similar conditions can be derived for the odd perturbations and more generally for combined perturbations. In the

calculations presented in this paper, we ensure that the perturbations we consider do not violate these no-signature change conditions, using the above analytic considerations for individual modes or equivalent numerical conditions for simulations with superpositions of modes. For the latter case, we ensure numerically that the signature of the metric does not change throughout the simulation outside an excision region (set at $r = 2.1$), and discontinue the integration of the geodesics if such a change occurs inside this excision region.

## IV. THE EFFECT OF METRIC PERTURBATIONS ON PHOTON PROPAGATION

In order to calculate the effect of metric perturbations on the propagation of photons in the vicinity of the black-hole horizon, we use the ray tracing algorithm described in Ref. [45], but with two important modifications. First, we rewrote the relevant expressions for the metric and for the Christoffel symbols in terms of the ingoing Eddington-Finkelstein coordinates we use here. Second, because the introduction of time-dependent, nonaxisymmetric perturbations removes all symmetries from the metric, we cannot use any of the Killing equations to integrate the null geodesics. Instead, we integrate directly the four second-order geodesic equations for the coordinates $u$, $r$, $\theta$, and $\phi$, with the Christoffel symbols evaluated analytically to linear order in the metric perturbations.

The ray tracing algorithm considers a Cartesian grid $(\alpha_0, \beta_0)$ on a virtual screen of an observer at infinity (the image plane) and solves using backwards evolution for the null geodesics of photon trajectories that cross the image plane with 3-momenta that are perpendicular to the screen. Using these geodesics, we define the shadow of the black hole as the locus of points on the image plane at which the corresponding null geodesics cross the event horizon of the black hole, when traced backwards [46,47]. When we calculate images using the thermodynamic properties of plasma that fills the black-hole spacetime, we integrate the radiative transfer equation along each null geodesic, neglecting the effects of scattering. For more details of the ray tracing algorithm see Refs. [45,48,49].

In order to understand the dependence of our results on the parameters of the spectrum of perturbations, we first explore some simple cases of monochromatic perturbations. Figure 1 shows a cross section of photon trajectories around a Schwarzschild black hole and compares them to those in a perturbed spacetime, in which we consider different phases of a single, spherically symmetric ($l = m = 0$) perturbation in the $vv$-component of the metric with an amplitude of $\epsilon_{vv}^{00} = \epsilon_{vv} = 0.5$, a radial extent of $R_{\rm G} = 1$, a frequency of $\omega = \omega_{\rm T} = (8\pi)^{-1}$, and a radial wavelength of $k_r = \omega_{\rm T}$. In all panels, the trajectories are colored blue if, in the absence of any perturbations, they would have crossed the event horizon and red otherwise. Clearly, the presence of perturbations affects the photon trajectories, causing some of the photons that would have crossed the horizon to escape and vice versa. This will significantly influence the shape and size of the shadow cast by the black hole on the surrounding emission. Moreover, the radial character of these perturbations causes light rays with different impact parameters to periodically bundle up and diverge, which will alter the brightness amplification introduced by gravitational lensing and lead to bright structures in the resulting images.

As Figs. 2 and 3 show, these qualitative properties of the photon trajectories in perturbed spacetimes remain the same when we introduce modes that are not spherically symmetric, or similar perturbations in the other components of the metric. In the latter case, we find that the amplitude of the effect is largest for perturbations to the $vv$-component of the metric. In fact, perturbing the $rv$-component of the metric has the smallest effect on the photon trajectories, at all phases of the oscillations. This is expected since it is the $vv$-component of the metric that primarily determines the magnitude of strong-field lensing experienced by the photons in the vicinity of the black hole.

Figure 4 shows the time dependence of the shadow cast by the black hole on the surrounding emission for the different phases of the spherically symmetric perturbation shown in Fig. 1. As expected, the size of the shadow is a strong function of the perturbation phase; the shape of the shadow remains circular because of the spherically symmetric character of the perturbations considered here (see, however, Fig. 5 for a more general axisymmetric case). The location and shape of the shadow are determined by the properties of the circular photon orbit, which is located at $r = 3$ in the unperturbed spacetime. The circular photon orbit is unstable since it corresponds to a local maximum in the effective potential for the photons. As a result, even small perturbations in the metric can significantly shift the location of the photon orbit and the effect will only be amplified by the gravitational lensing that photons experience as they travel from the vicinity of the black hole to the observer at infinity. In particular, note that we have set $\epsilon_{vv} = 0.5$ and the perturbation of the metric at the location of the photon orbit has a magnitude of only $\epsilon_{vv} \exp[-(3-2)^2/2] \simeq 0.3$. Even then, the net result is a large periodic fluctuation of the diameter of the black-hole shadow that, in this case, ranges from $6M$ (lower right panel) to $12M$ (lower left panel).

In order to explore the dependence of the average black-hole shadows on the various parameters that describe the metric perturbations, we define the average opaqueness of a given location on the observer's image plane as the fraction of the perturbation period during which this location is within the perimeter of the instantaneous shadow. For the case of the spherically symmetric perturbations of Fig. 1, the average opaqueness depends only on the distance from the center of the black-hole shadow and is shown for different values of the parameters of the perturbation in

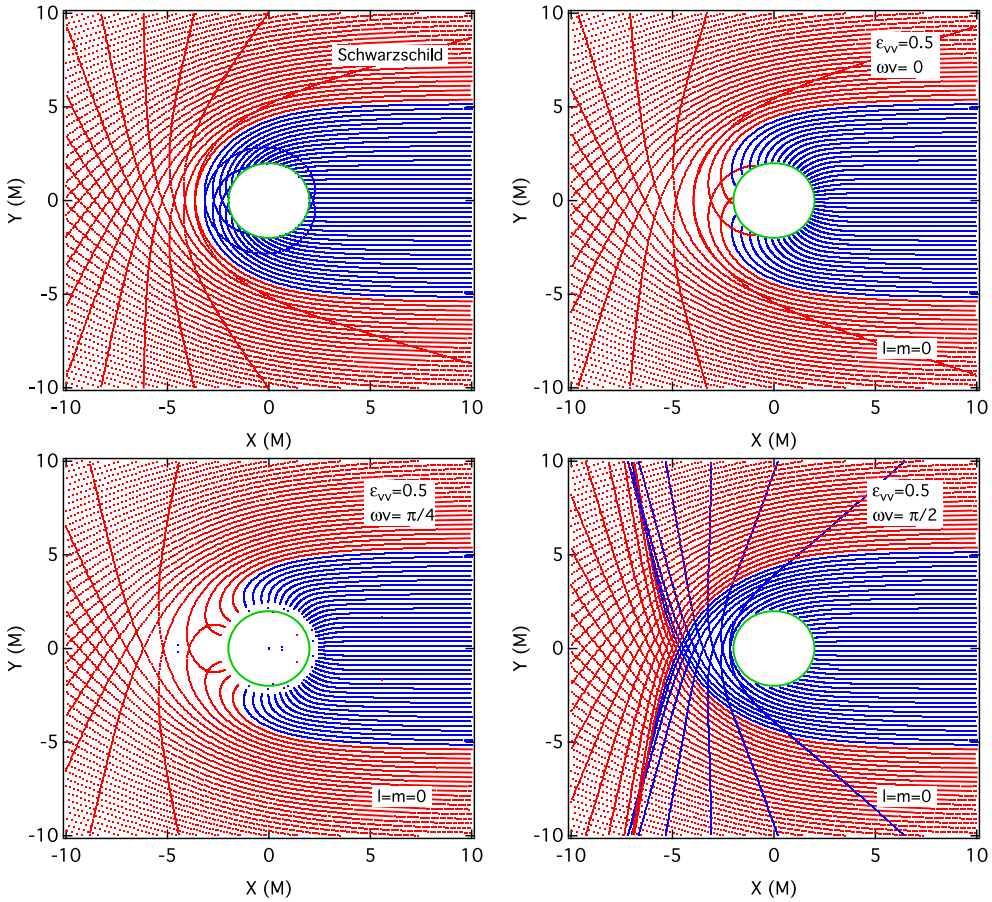


FIG. 1. The trajectories of photons approaching a nonspinning black hole in plane parallel rays from far infinity (from the right side of the figure). The upper left panel shows the trajectories around an unperturbed Schwarzschild black hole. The other panels correspond to different phases of a black hole with a single, spherically symmetric metric perturbation (see text for details). In all panels, photon trajectories are colored blue if (in the absence of any perturbations) they would have crossed the event horizon and are colored red if they would have escaped to infinity. As expected, metric perturbations cause some of the blue trajectories to escape to infinity and some of the red trajectories to cross the event horizon, at different phases of the perturbation.

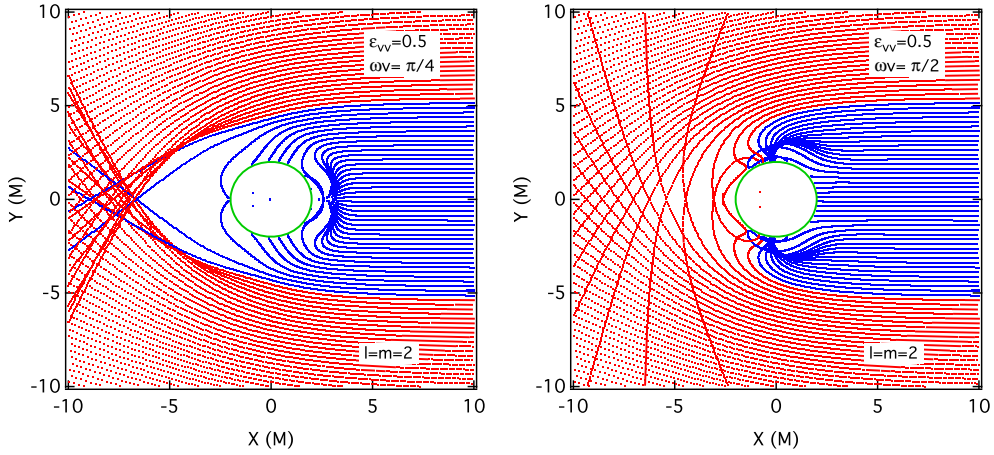


FIG. 2. Same as in Fig. 1 but for two phases of an $l = m = 2$ perturbation mode. All other parameters remain the same.

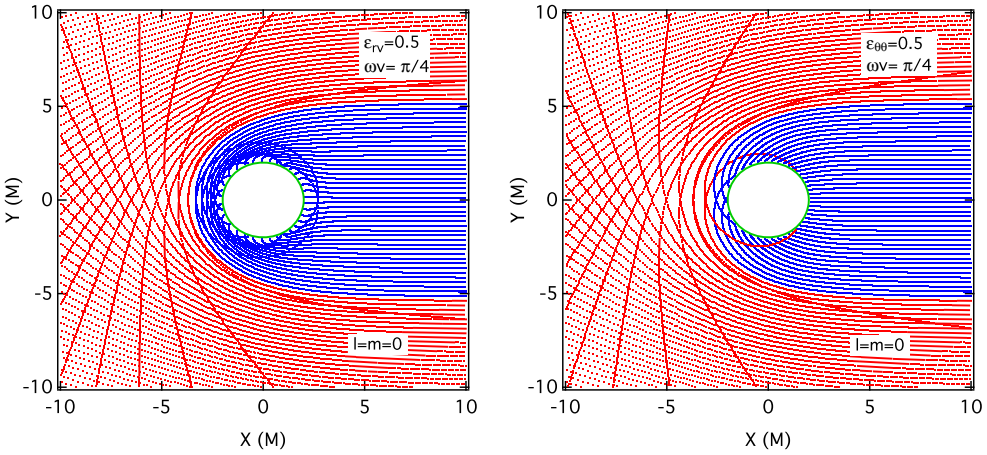


FIG. 3. Same as in Fig. 1 but for perturbing only the *(left)* $rv$- and *(right)* $\theta\theta$-components of the metric. All other parameters remain the same. The effects of perturbing different components of the metric are all qualitatively similar to those shown in Fig. 1 for the $vv$-component.

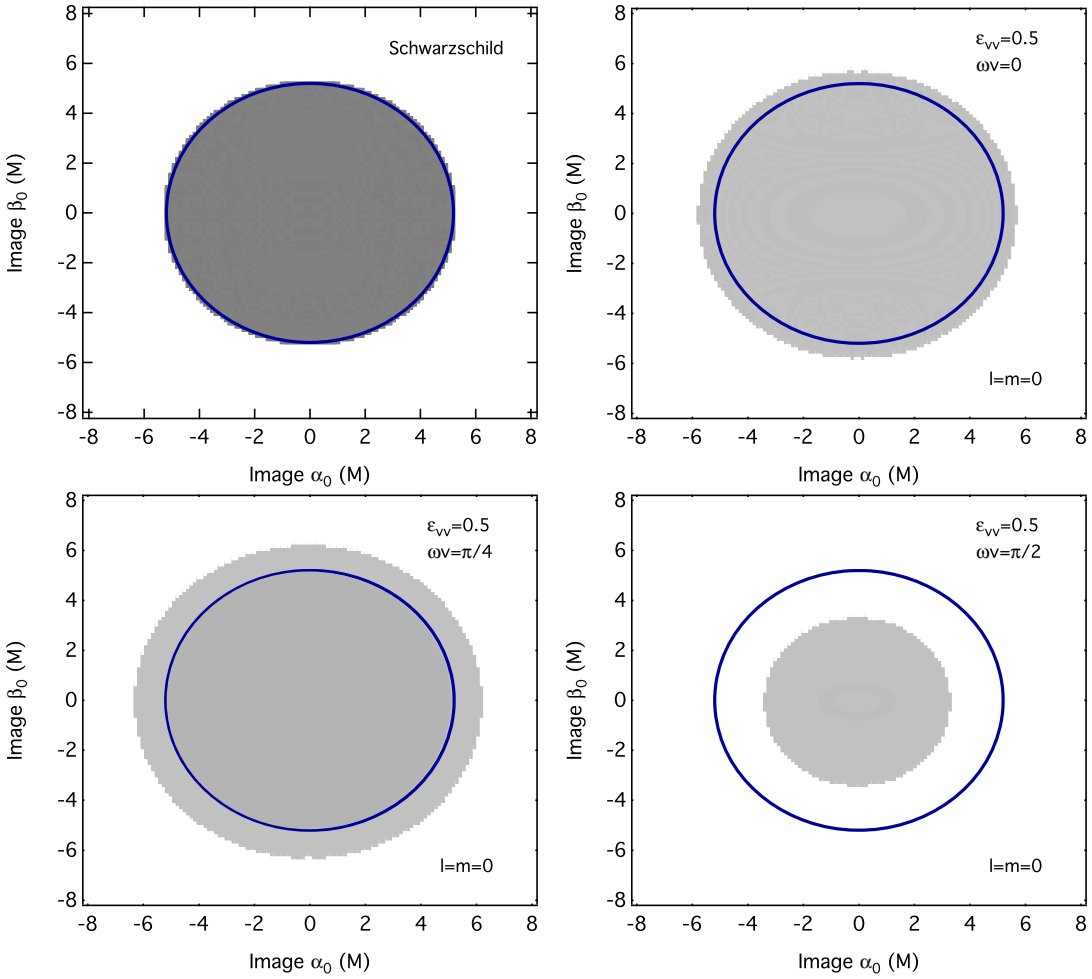


FIG. 4. The shadows of the black holes that correspond to the four configurations shown in Fig. 1. In all panels, the blue circle shows the outline of the unperturbed Schwarzschild black hole. For the perturbed black hole, the size of the shadow is time-dependent and can be significantly different from the Schwarzschild case.

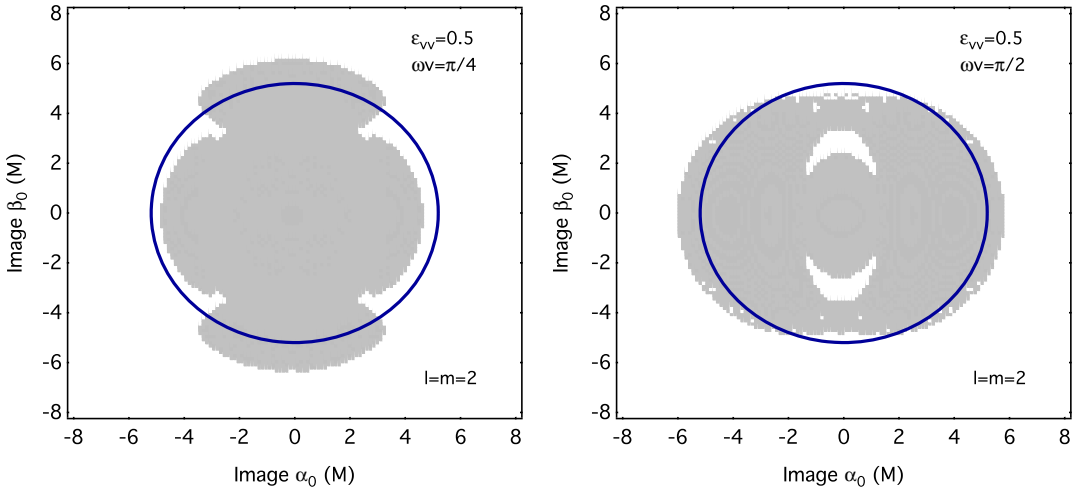


FIG. 5. Same as in Fig. 4 but for two phases of an $l = m = 2$ perturbation mode.

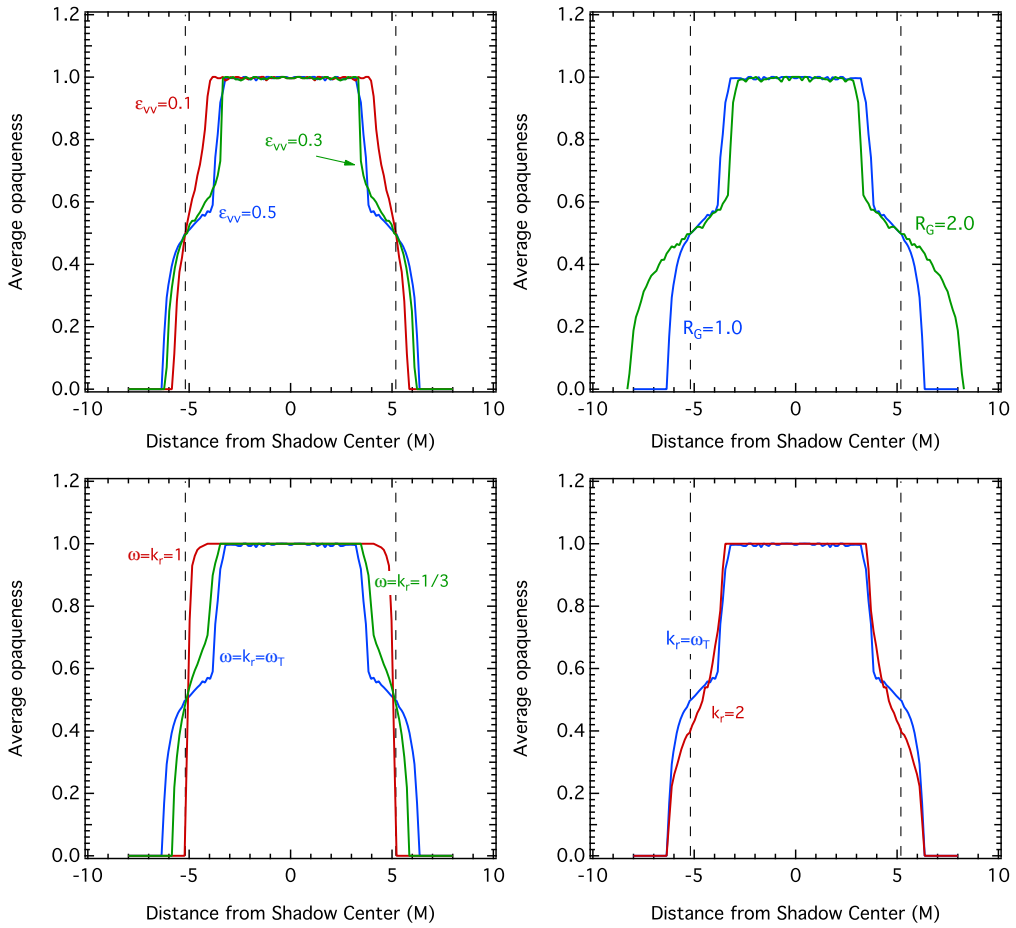


FIG. 6. The dependence of the average opaqueness of the black-hole shadow (as defined in the text) on *(upper left)* the amplitude, *(upper right)* the range, *(lower left)* the frequency, and *(lower right)* the wavelength of the perturbations. In all panels, the vertical dashed line shows the location of the shadow for the unperturbed black hole and the values of the parameters not shown are the same as in Fig. 1. Introducing perturbations to the black-hole metric causes the black-hole shadow to lose its sharpness and become blurry. The effect is larger for perturbations that are strong, slow, and that extend to a large distance from the event horizon.

Fig. 6. The radius of the photon orbit ($r = 3$) in the unperturbed metric and the light crossing time that corresponds to this length ($\delta v = 3$) set the optimal lengths and frequencies for the perturbations with maximal effects on the black-hole shadow. Indeed, the changes in the black-hole shadow become appreciable for order unity perturbations in the metric ($\epsilon_{vv} \gtrsim 0.1$), for radial extent of order the horizon scale ($R_{\rm G} \gtrsim 1$), and for relatively slow angular frequencies ($\omega \lesssim 1$). Perturbations with smaller amplitudes that are confined too close to the horizon do not affect the propagation of the photons in the vicinity of the photon radius and hence have no appreciable effect on the black-hole shadow. This is also true for perturbations that are too fast compared to the light crossing time for the photon orbit, since their effects average out during the passage of the photons across the region that determines the black-hole shadow. Finally, as expected, the radial wavelength of the perturbations alters the radial dependence of the opaqueness as it determines the details of the metric perturbations within the envelope described by the range $R_{\rm G}$.

## V. IMAGES OF ACCRETION FLOWS

In this section, we explore the effect of the metric perturbations discussed in Sec. III on the expected images of accretion flows that will be obtained by the Event Horizon Telescope. Following Ref. [50], we consider the simplest possible plasma model for the accretion flow that preserves the main characteristics of images from more complicated GRMHD simulations (see, e.g., [49,51–54]).

The millimeter radiation observed from the main EHT targets is the result of nearly optically thin synchrotron emission from thermal electrons from a horizon-sized region in the accretion flow. The monochromatic emissivity of synchrotron emission scales as $j \sim n_e B^2$, where $n_e$ and $B$ are the electron density and magnetic field of the region, respectively. The magnetic field is in near equipartition with the plasma and, therefore, $B \sim n_e^{1/2}$. As a result, the monochromatic emissivity scales as $j \sim n_e^2$.

Radiatively inefficient accretion models for the main EHT targets suggest that the electron density in the inner flow region scales as $n_e \sim r^{-1}$ (see [50] and references therein), which we assume here. We also set the 4-velocity of the plasma outside the location of the innermost stable circular orbit of the unperturbed metric to the orbital velocity at the projected cylindrical radius $\varpi = r \sin\theta$, i.e.,

$$(u^v, u^r, u^\theta, u^\phi) = \left(\sqrt{\frac{\varpi}{\varpi - 3}}, 0, 0, \frac{1}{\varpi\sqrt{\varpi - 3}}\right). \quad (15)$$

In the plunging region inside the innermost stable circular orbit, we set the plasma 4-velocity to the local free fall velocity of the unperturbed metric. We also set the local electron density such that the mass accretion rate in the plunging region is constant, i.e., such that

$$(n_{\rm e} u^\mu)_{;\mu} = 0. \quad (16)$$

In all the above, we are making the assumption that the plasma properties are not affected by the metric perturbations. Even though we make this assumption purely for simplicity, it is also justified by the fact that most of the emission comes from radii $r > 6$ at which the metric perturbations are exponentially very small (i.e., $\exp(-8) \simeq 3 \times 10^{-4}$).

The upper left panel of Fig. 7 shows the predicted image from this simplified model for an unperturbed Schwarzschild metric, as viewed by an observer at the equatorial plane of our coordinate system. The image is not spherically symmetric because of the cylindrical character of the plasma orbits and is dominated by the Doppler boosted crescent of emission from the plasma with velocities pointing towards the distant observer. It also shows the outline of the black-hole shadow and a faint photon ring surrounding it. The remaining panels of the figure show the images during different phases of a perturbation with the same parameters as those shown in Fig. 1.

As discussed in Sec. IV, the main effect of the metric perturbation is to alter the location of the photon orbit and hence the size of the shadow cast by the black hole on the surrounding emission. Moreover, the radial wavelength of the perturbations causes trajectories with different impact parameters to bundle up and this leads to pronounced bright structures, such as the bright ring surrounding the shadow (compare, e.g., the lower right panels of Figs. 1 and 7).

The presence of modes that are not spherically symmetric further distorts the image of the accretion flow. Two example phases are shown in Fig. 8 for an $l = m = 2$ mode with all the other parameters being the same as for the $l = m = 0$ mode shown in Fig. 7.

More realistic situations are, of course, expected to require us to consider a superposition of oscillatory modes with different amplitudes, frequencies, phases, and wave numbers. This superposition will break the symmetries as well as the purely periodic character of the images shown in Figs. 7 and 8. Moreover, it is possible that the lack of symmetry might suppress the magnitude of the effect on the images. Exploring the implications for the predicted images from different spectra of perturbations is beyond the scope of this initial study. However, in order to get a first look into the effect of the superposition of different modes, we performed a calculation with a small number of modes with properties summarized in Table I. The amplitudes, frequencies, wavelengths, and phases of these modes were chosen rather arbitrarily, with the requirement that the frequencies and wavelengths are noncommensurate.

Figure 9 shows the images calculated during four instances in the evolution of the mode spectrum shown in Table I. The lack of symmetry in the images is

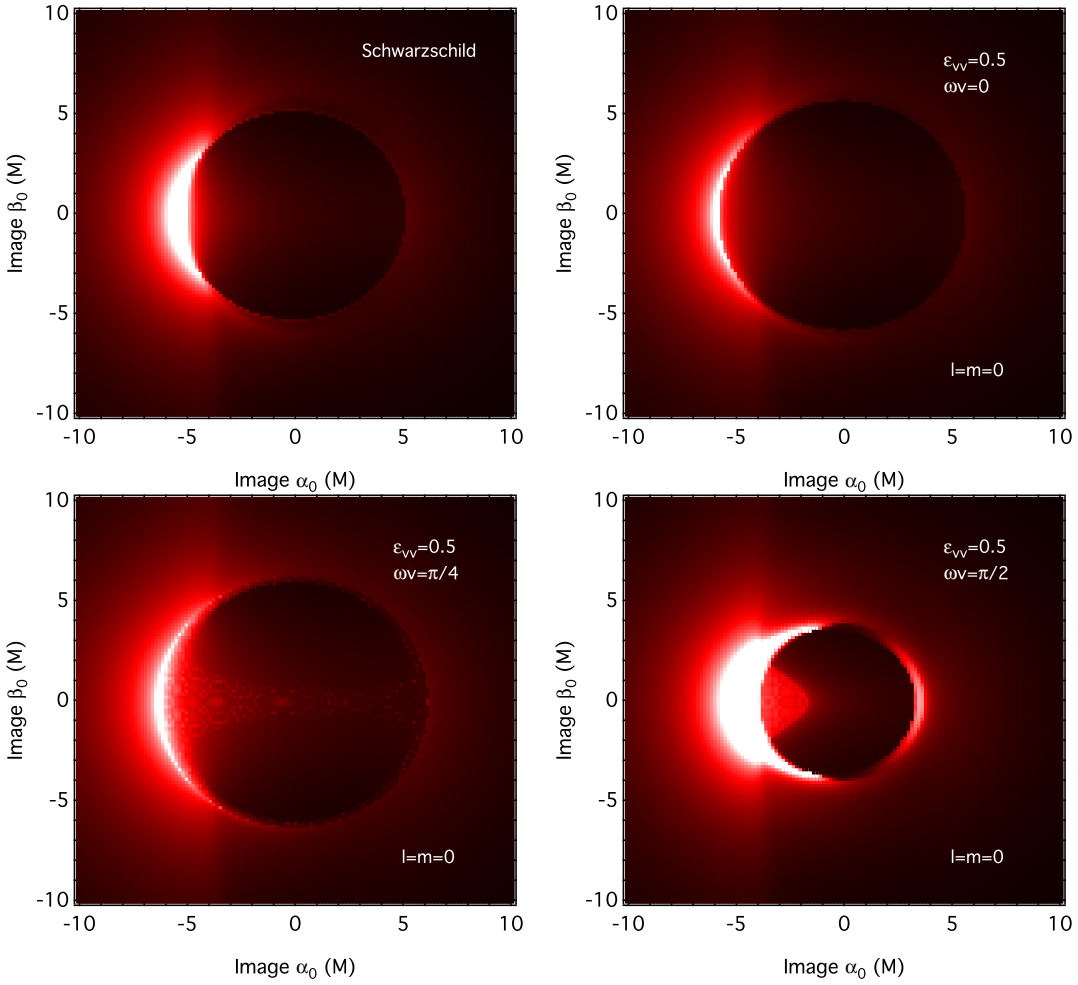


FIG. 7. Same as Fig. 4 but with images from a simple plasma model for the emission from the inner accretion flow. The metric perturbations change in a time-dependent manner the image of the flow as well as the size, brightness, and width of the bright photon ring that surrounds the black-hole shadow.

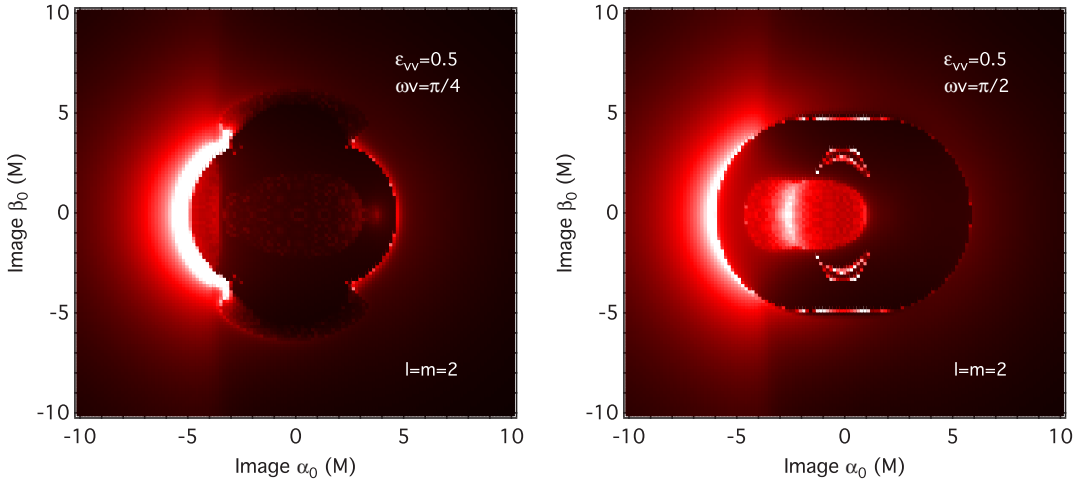


FIG. 8. Same as Fig. 7 but for two phases of an $l = m = 2$ perturbation mode.

TABLE I. Properties of sample spectrum of metric perturbations.

| Mode | $lm$ | Amplitude | Phase$/2\pi$ | $\omega/\omega_{\rm T}$ | $k/\omega_{\rm T}$ |
|---|---|---|---|---|---|
| $vv$ | 00 | 0.9 | 0.0 | 1 | $\pi/4$ |
| $vv$ | 21 | 1.0 | 0.2 | $\pi/4$ | $\sqrt{2}$ |
| $rr$ | 00 | 1.1 | $\sqrt{2}$ | $\sqrt{2}$ | 1.1 |
| $rr$ | 11 | $\pi/3$ | 1.2 | 0.9 | 0.8 |
| $rv$ | 10 | $\pi/4$ | 0.3 | 1.1 | 0.9 |
| $rv$ | 20 | $\sqrt{2}$ | 0.7 | 0.8 | $\pi/3$ |
| $\theta\theta$ | 10 | 1.2 | $\sqrt{5}/2$ | $\pi/3$ | $\sqrt{5}/2$ |
| $r$ (odd) | 21 | $\sqrt{5}/2$ | 0.1 | 1.0 | $\pi/3$ |
| $v$ (odd) | 11 | 1.0 | 0.5 | 0.95 | 1.0 |

evident. Moreover, the superposition of modes does not suppress the effect of individual modes on the images but rather exaggerates it. Indeed, the black-hole shadow shape becomes highly asymmetric and rapidly fluctuating and its characteristic "size" shows order unity variability.

Figures 10 and 11 show the effect of changing the overall amplitudes and the characteristic frequencies of the spectrum of perturbations. As expected from the discussion of the results presented in Fig. 6, moderate reduction of the amplitude of perturbations does not introduce qualitative differences in the resulting images; the outline of the black-hole shadow is determined by the size and shape of the unstable photon orbits, which can be altered substantially even with moderately small metric perturbations. (Figure 6 suggests significant differences after an order-of-magnitude reduction.) On the other hand, increasing the frequencies of the modes reduces the magnitude of the effect on the images, because the rapid oscillations of the various metric elements are averaged out during the time it takes for photons to cross distances comparable to the radius of the photon orbit.

Figure 12 shows the average image of the simulations shown in Fig. 9 calculated between the times $v = 0$ and $v = 32(2\pi/\omega_{\rm T})$. As expected, the rapid variability of the images leads to a blurry black-hole shadow that is difficult to discern.

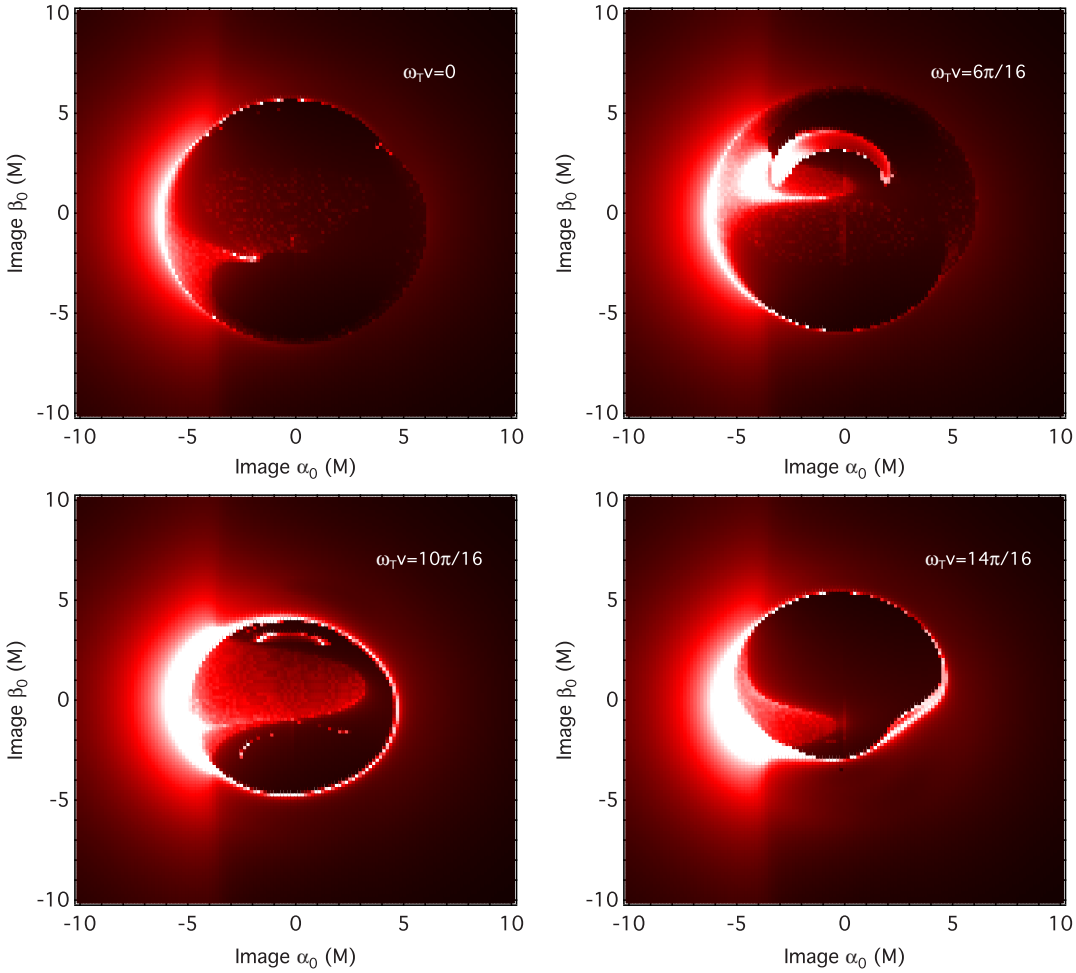


FIG. 9. Four images of the accretion flow around a black hole at different instants with the spectrum of metric perturbations given in Table I. The superposition of modes causes the shape and size of the black-hole shadow to be highly asymmetric and variable.

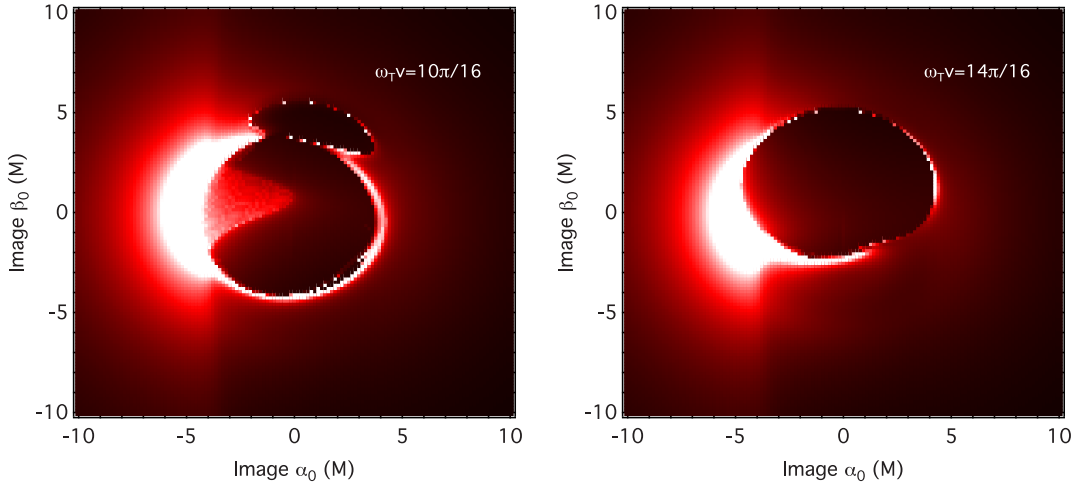


FIG. 10. Same as Fig. 9 but for all mode amplitudes reduced by a factor of three.

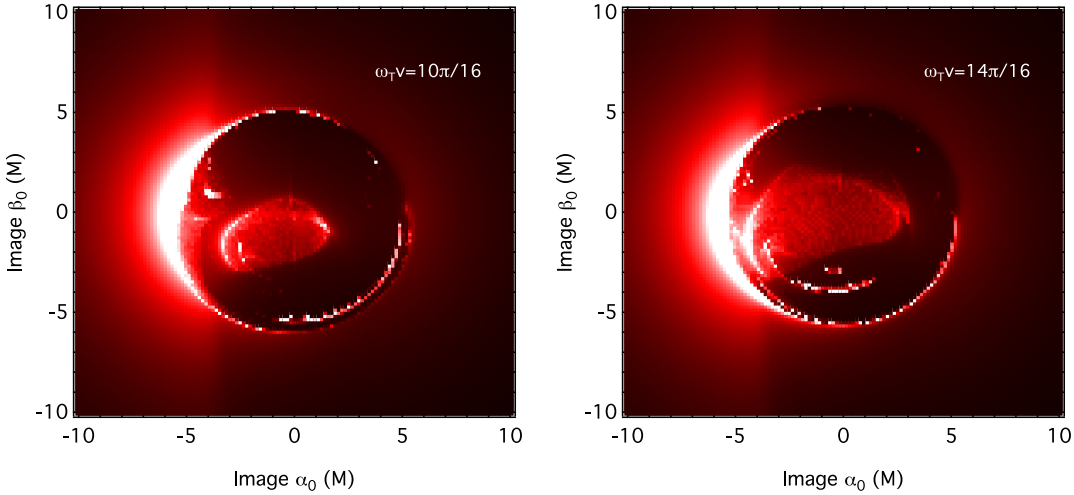


FIG. 11. Same as Fig. 9 but with all frequencies scaled by artificially increasing to $\omega_{\mathrm{T}} = 1$.

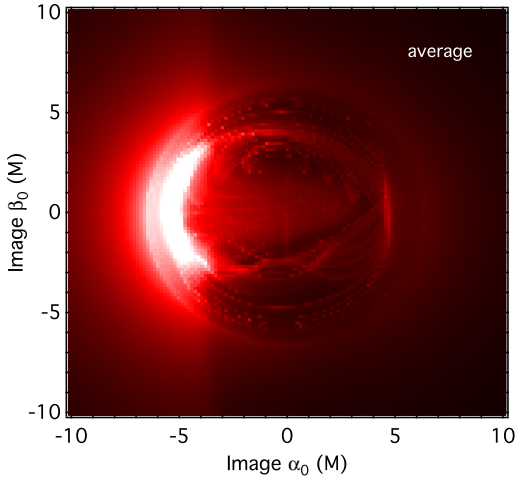


FIG. 12. The average image for a black hole with the spectrum of metric perturbations given in Table I calculated between the times $v = 0$ and $v = 32(2\pi/\omega_{\mathrm{T}})$. The net effect of averaging is a blurry black-hole shadow that is difficult to discern.

## VI. IMPLICATIONS FOR EVENT HORIZON TELESCOPE OBSERVATIONS

In the last two sections, we showed that horizon-scale perturbations in the spacetime of an astrophysical black hole introduce a significant, time-dependent variation of the size and shape of the shadow it casts on the surrounding emission, as well as bright structures, such as rings of emission, that are also time dependent. As discussed in Sec. II, we considered a characteristic frequency of these oscillations that is of order $\omega_T = (8\pi M)^{-1}$ and which, therefore, depends on the mass of the black hole under study.

There are two primary targets for the Event Horizon Telescope: the black hole in the center of the Milky Way, Sgr A*, and the black hole in the center of the M87 galaxy. The former has a mass of $\sim 4.3 \times 10^6\ M_\odot$ [55,56] while the latter is $\sim$1500 times more massive at $\sim 6.5 \times 10^9\ M_\odot$ [57]. Even though it remains to be determined whether a clearly visible black-hole shadow is cast on their 1.3 mm images,

early EHT observations of both targets have demonstrated that the image sizes are comparable to their horizons [58,59].

Introducing physical units back to the dimensionless expressions, the characteristic period of the metric perturbations becomes

$$P \simeq \frac{2\pi}{\omega_{\mathrm{T}}} = \simeq 0.93\left(\frac{M}{4.3\times 10^{6}\ M_{\odot}}\right)\ \mathrm{hr} \simeq 59\left(\frac{M}{6.5\times 10^{9}\ M_{\odot}}\right)\ \mathrm{d}, \quad (17)$$

where the first of the two estimates corresponds to Sgr A* and the second to M87. These are the timescales at which the black-hole shadows will change, if quantum fluctuations such as the ones we consider here are present.

The Event Horizon Telescope uses the rotation of the Earth to increase the coverage of the interferometric $u-v$ plane and construct an image. Each imaging observation will require scanning the $u-v$ plane over a period of several hours. In the case of Sgr A*, the timescale of metric perturbations is comparable to or shorter than each imaging scan and, therefore, individual snapshots of the effect of metric perturbations on the images will not be generated. Moreover, because of the particular interferometric methods used in the Event Horizon Telescope (as in all mm VLBI experiments), the images generated using multi-hour scans of the $u-v$ plane will not be simple averages of the actual images, such as the one shown in Fig. 12. This is because the Event Horizon Telescope measures separately the magnitudes of the Fourier components of the individual snapshots and the closure phases of the same Fourier components along triangles of baselines, neither of which is the result of linear operations on the images.

Different sources of variability in the black-hole image such as those introduced by the turbulent accretion flow [60,61], by refractive scattering in the interstellar medium [62], as well as by the metric perturbations we discuss here, will imprint different signatures on the interferometric visibilities. Nonimaging techniques such as those discussed in Ref. [63] will need to be employed to distinguish and identify the signatures of metric perturbations from other sources of variability. Distinguishing characteristics of the metric perturbations that we consider include the fact that they decay very quickly away from the horizon. This causes them to alter primarily the outline of the black-hole shadow without introducing significant variability in the bulk of the emission, which originates outside the radius of the innermost stable circular orbit. Moreover, only metric perturbations are achromatic, i.e., they affect photons of all wavelengths in the same way. In the near future, the Event Horizon Telescope will operate at two different wavelengths (1.3 mm and 0.8 mm). Comparison of the image variability at these two wavelengths will be important in separating the effects of perturbations in the geometry of spacetime from those introduced by variability in the plasma.

In the case of M87, the assumed timescale of metric perturbations is longer than a single imaging scan and, therefore, images constructed in different observing epochs (days) will correspond to different snapshots of the perturbations. Moreover, the lack of appreciable image blurring due to scattering in the interstellar medium towards M87 will allow for measuring the size and shape of the black-hole shadow in that source without a need for additional corrections. Both these properties make the black hole in M87 the optimal candidate for searching for black-hole quantum structure with the Event Horizon Telescope.

If evidence of perturbations like those considered here is found in EHT observations, there is no apparent explanation within classical GR. Thus, this would strongly indicate phenomena well-outside a general-relativistic description, with a prime candidate being quantum black-hole structure associated with the need to make black holes consistent with quantum mechanics.

## ACKNOWLEDGMENTS

We wish to thank S. Britzen, D. Marolf, and F. Özel, for helpful discussions. The work of S. G. was supported in part by the U.S. DOE under Contract No. DE-SC0011702 and by Foundational Questions Institute (fqxi.org) Grant No. FQXi-RFP-1507. The work of D. P. was supported in part by NASA TCAN award NNX14AB48G and by NSF Grant No. AST 1312034.

[1] S. W. Hawking, Particle creation by black holes, Commun. Math. Phys. **43**, 199 (1975); **46**, 206(E) (1976).
[2] J. Preskill, Do black holes destroy information?, in International Symposium on Black holes, Membranes, Wormholes and Superstrings Woodlands, Texas, 1992, arXiv:hep-th/9209058.
[3] D. N. Page, Black hole information, in 5th Canadian Conference on General Relativity and Relativistic Astrophysics (5CCGRRA) Waterloo, Canada, 1993, arXiv:hep-th/9305040.
[4] S. B. Giddings, Quantum mechanics of black holes, in High-Energy Physics and Cosmology. Proceedings, Summer School, Trieste, Italy, 1994, arXiv:hep-th/9412138.

[5] S. D. Mathur, The information paradox: A pedagogical introduction, Classical Quantum Gravity **26**, 224001 (2009).
[6] S. B. Giddings, Black holes, quantum information, and the foundations of physics, Phys. Today **66**, 30 (2013).
[7] D. Harlow, Jerusalem lectures on black holes and quantum information, Rev. Mod. Phys. **88**, 015002 (2016).
[8] S. B. Giddings, Black holes and massive remnants, Phys. Rev. D **46**, 1347 (1992).
[9] S. D. Mathur, Fuzzballs and the information paradox: A summary and conjectures, arXiv:0810.4525.
[10] P. O. Mazur and E. Mottola, Gravitational vacuum condensate stars, Proc. Natl. Acad. Sci. U.S.A. **101**, 9545 (2004).
[11] A. Almheiri, D. Marolf, J. Polchinski, and J. Sully, Black holes: Complementarity or firewalls?, J. High Energy Phys. 02 (2013) 062.
[12] J. Maldacena and L. Susskind, Cool horizons for entangled black holes, Fortschr. Phys. **61**, 781 (2013).
[13] S. B. Giddings, Possible observational windows for quantum effects from black holes, Phys. Rev. D **90**, 124033 (2014).
[14] N. Warner, Black Holes and Microstate Geometries, *Talk at Southern California Strings Seminar*, http://online.kitp.ucsb.edu/online/scss16/warner.
[15] S. B. Giddings, Models for unitary black hole disintegration, Phys. Rev. D **85**, 044038 (2012).
[16] S. B. Giddings, Black holes, quantum information, and unitary evolution, Phys. Rev. D **85**, 124063 (2012).
[17] S. B. Giddings, Nonviolent nonlocality, Phys. Rev. D **88**, 064023 (2013).
[18] S. B. Giddings, Observational strong gravity and quantum black hole structure, Int. J. Mod. Phys. D **25**, 1644014 (2016).
[19] D. Psaltis, Probes and tests of strong-field gravity with observations in the electromagnetic spectrum, Living Rev. Relativity **11**, 9 (2008).
[20] K. Nandra, D. Barret, X. Barcons, A. Fabian, J.-W. den Herder, L. Piro, M. Watson, C. Adami, J. Aird, J. M. Afonso *et al.*, The hot and energetic universe: A white paper presenting the science theme motivating the Athena+ mission, arXiv:1306.2307.
[21] B. P. Abbott, R. Abbott, T. D. Abbott, M. R. Abernathy, F. Acernese, K. Ackley, C. Adams, T. Adams, P. Addesso, R. X. Adhikari *et al.*, Observation of Gravitational Waves from a Binary Black Hole Merger, Phys. Rev. Lett. **116**, 061102 (2016).
[22] P. A. Seoane, S. Aoudia, H. Audley, G. Auger, S. Babak, J. Baker, E. Barausse, S. Barke, M. Bassan, V. Beckmann, M. Benacquista, P. L. Bender, E. Berti, P. Binétruy, J. Bogenstahl *et al.* (eLisa Consortium), The gravitational Universe, arXiv:1305.5720.
[23] S. Doeleman, E. Agol, D. Backer, F. Baganoff, G. C. Bower, A. Broderick, A. Fabian, V. Fish, C. Gammie, P. Ho, M. Honman, T. Krichbaum, A. Loeb, D. Marrone, M. Reid *et al.*, Imaging an event horizon: submm-VLBI of a super massive black hole, Astronomy **2010**, 68 (2009) [arXiv:0906.3899].
[24] S. B. Giddings, Gravitational wave tests of quantum modifications to black hole structure—with post-GW150914 update, Classical Quantum Gravity **33**, 235010 (2016).
[25] T. Johannsen, Systematic study of event horizons and pathologies of parametrically deformed Kerr spacetimes, Phys. Rev. D **87**, 124017 (2013).
[26] T. Regge and J. A. Wheeler, Stability of a Schwarzschild singularity, Phys. Rev. **108**, 1063 (1957).
[27] T. Johannsen and D. Psaltis, Testing the no-hair theorem with observations in the electromagnetic spectrum. II. Black hole images, Astrophys. J. **718**, 446 (2010).
[28] C. Bambi and N. Yoshida, Shape and position of the shadow in the $\delta = 2$ Tomimatsu-Sato spacetime, Classical Quantum Gravity **27**, 205006 (2010).
[29] A. Abdujabbarov, F. Atamurotov, Y. Kucukakca, B. Ahmedov, and U. Camci, Shadow of Kerr-Taub-NUT black hole, Astrophys. Space Sci. **344**, 429 (2013).
[30] L. Amarilla and E. F. Eiroa, Shadow of a Kaluza-Klein rotating dilaton black hole, Phys. Rev. D **87**, 044057 (2013).
[31] F. H. Vincent, E. Gourgoulhon, C. Herdeiro, and E. Radu, Astrophysical imaging of Kerr black holes with scalar hair, Phys. Rev. D **94**, 084045 (2016).
[32] P. Hayden and J. Preskill, Black holes as mirrors: Quantum information in random subsystems, J. High Energy Phys. 09 (2007) 120.
[33] S. B. Giddings and Y. Shi, Quantum information transfer and models for black hole mechanics, Phys. Rev. D **87**, 064031 (2013).
[34] L. Susskind, The transfer of entanglement: The case for firewalls, arXiv:1210.2098.
[35] S. B. Giddings, Nonviolent information transfer from black holes: A field theory parametrization, Phys. Rev. D **88**, 024018 (2013).
[36] S. B. Giddings and Y. Shi, Effective field theory models for nonviolent information transfer from black holes, Phys. Rev. D **89**, 124032 (2014).
[37] D. N. Page, Average Entropy of a Subsystem, Phys. Rev. Lett. **71**, 1291 (1993).
[38] D. N. Page, Information in Black Hole Radiation, Phys. Rev. Lett. **71**, 3743 (1993).
[39] S. B. Giddings, Statistical physics of black holes as quantum-mechanical systems, Phys. Rev. D **88**, 104013 (2013).
[40] V. P. Frolov and D. Fursaev, Mining energy from a black hole by strings, Phys. Rev. D **63**, 124010 (2001).
[41] V. P. Frolov, Cosmic strings and energy mining from black holes, Int. J. Mod. Phys. A **17**, 2673 (2002).
[42] A. E. Lawrence and E. J. Martinec, Black hole evaporation along macroscopic strings, Phys. Rev. D **50**, 2680 (1994).
[43] A. R. Brown, Tensile Strength and the Mining of Black Holes, Phys. Rev. Lett. **111**, 211301 (2013).
[44] S. B. Giddings, Modulated Hawking radiation and a nonviolent channel for information release, Phys. Lett. B **738**, 92 (2014).
[45] D. Psaltis and T. Johannsen, A ray-tracing algorithm for spinning compact object spacetimes with arbitrary quadrupole moments. I. Quasi-Kerr black holes, Astrophys. J. **745**, 1 (2012).
[46] J. M. Bardeen, Timelike and null geodesics in the Kerr metric, in *Black Holes (Les Astres Occlus)*, edited by C. Dewitt and B. S. Dewitt (Gordon and Breach, New Yok, 1973), pp. 215–239.

[47] J.-P. Luminet, Image of a spherical black hole with thin accretion disk, Astron. Astrophys. **75**, 228 (1979).
[48] C.-k. Chan, D. Psaltis, and F. Özel, GRay: A massively parallel GPU-based code for ray tracing in relativistic spacetimes, Astrophys. J. **777**, 13 (2013).
[49] C.-K. Chan, D. Psaltis, F. Özel, R. Narayan, and A. Sadowski, The power of imaging: Constraining the plasma properties of GRMHD simulations using EHT observations of Sgr A*, Astrophys. J. **799**, 1 (2015).
[50] A. E. Broderick, T. Johannsen, A. Loeb, and D. Psaltis, Testing the no-hair theorem with Event Horizon Telescope observations of Sagittarius A*, Astrophys. J. **784**, 7 (2014).
[51] J. Dexter, E. Agol, and P. C. Fragile, Millimeter flares and VLBI visibilities from relativistic simulations of magnetized accretion onto the galactic center black hole, Astrophys. J. **703**, L142 (2009).
[52] J. Dexter, E. Agol, P. C. Fragile, and J. C. McKinney, The submillimeter bump in Sgr A* from relativistic MHD simulations, Astrophys. J. **717**, 1092 (2010).
[53] M. Mościbrodzka, C. F. Gammie, J. C. Dolence, H. Shiokawa, and P. K. Leung, Radiative models of SGR A* from GRMHD simulations, Astrophys. J. **706**, 497 (2009).
[54] M. Mościbrodzka, H. Falcke, H. Shiokawa, and C. F. Gammie, Observational appearance of inefficient accretion flows and jets in 3D GRMHD simulations: Application to Sagittarius A*, Astron. Astrophys. **570**, A7 (2014).
[55] A. M. Ghez, S. Salim, N. N. Weinberg, J. R. Lu, T. Do, J. K. Dunn, K. Matthews, M. R. Morris, S. Yelda, E. E. Becklin, T. Kremenek, M. Milosavljevic, and J. Naiman, Measuring distance and properties of the Milky Way's central supermassive black hole with stellar orbits, Astrophys. J. **689**, 1044 (2008).
[56] S. Gillessen, F. Eisenhauer, S. Trippe, T. Alexander, R. Genzel, F. Martins, and T. Ott, Monitoring stellar orbits around the massive black hole in the Galactic Center, Astrophys. J. **692**, 1075 (2009).
[57] K. Gebhardt, J. Adams, D. Richstone, T. R. Lauer, S. M. Faber, K. Gültekin, J. Murphy, and S. Tremaine, The black hole mass in M87 from Gemini/NIFS adaptive optics observations, Astrophys. J. **729**, 119 (2011).
[58] S. S. Doeleman, J. Weintroub, A. E. E. Rogers, R. Plambeck, R. Freund, R. P. J. Tilanus, P. Friberg, L. M. Ziurys, J. M. Moran, B. Corey, K. H. Young, D. L. Smythe, M. Titus, D. P. Marrone, R. J. Cappallo *et al.*, Event-horizon-scale structure in the supermassive black hole candidate at the Galactic Centre, Nature (London) **455**, 78 (2008).
[59] S. S. Doeleman, V. L. Fish, D. E. Schenck, C. Beaudoin, R. Blundell, G. C. Bower, A. E. Broderick, R. Chamberlin, R. Freund, P. Friberg, M. A. Gurwell, P. T. P. Ho, M. Honma, M. Inoue, T. P. Krichbaum *et al.*, Jet-launching structure resolved near the supermassive black hole in M87, Science **338**, 355 (2012).
[60] R.-S. Lu, F. Roelofs, V. L. Fish, H. Shiokawa, S. S. Doeleman, C. F. Gammie, H. Falcke, T. P. Krichbaum, and J. A. Zensus, Imaging an event horizon: Mitigation of source variability of Sagittarius A*, Astrophys. J. **817**, 173 (2016).
[61] L. Medeiros, C.-k. Chan, F. Ozel, D. Psaltis, J. Kim, D. P. Marrone, and A. Sadowski, GRMHD simulations of visibility amplitude variability for Event Horizon Telescope images of Sgr A*, arXiv:1601.06799.
[62] M. D. Johnson and C. R. Gwinn, Theory and simulations of refractive substructure in resolved scatter-broadened images, Astrophys. J. **805**, 180 (2015).
[63] S. S. Doeleman, V. L. Fish, A. E. Broderick, A. Loeb, and A. E. E. Rogers, Detecting flaring structures in Sagittarius A* with high-frequency VLBI, Astrophys. J. **695**, 59 (2009).